JMEPEG (2023) 32:9344–9356
https://doi.org/10.1007/s11665-022-07775-4

1059-9495/$19.00

TECHNICAL ARTICLE

Influence of Extrusion Temperature on the Microstructure and Mechanical Properties of a 0.5 wt.% Graphene Nanoplatelet-Reinforced Aluminum Composite

Shumei Lou, Baojia Cheng, Yongqiang Liu, Xin Li, Xuefeng Bai, Peng Chen, Yiming Li, and Li Li

Submitted: 2 June 2022 / Revised: 29 October 2022 / Accepted: 23 November 2022 / Published online: 27 December 2022

In this study, hot extrusions at 460, 470, 480, 490, and 500 °C were carried out on 0.5 wt.% graphene nanoplatelet-reinforced aluminum (0.5 wt.% GNPs /Al) composite prepared by powder metallurgy and hot pressing. The microstructure and mechanical properties of hot extruded composite were investigated. The reinforcement effect of hot extrusion on GNPs/Al composite is the synthetic actions of work hardening, dynamic recovery and dynamic recrystallization of matrix grains, and the dispersion, delamination and structure of the GNPs in the composite due to the different fluidity of the matrix at different temperatures. As a result, the comprehensive mechanical properties of the composite extruded at 490 °C are the best. The TEM image exhibits that, at the optimal extrusion temperature of 490 °C, GNPs are uniformly distributed in the aluminum matrix, mainly dispersed at the grain boundaries, where some Al_4C_3 and Al_2O_3 exhibit pinning effects to form fine interface between the GNPs and the matrix.

Keywords 0.5 wt.% GNPs/Al composite, extrusion temperature, hot extrusion, mechanical properties, microstructure

1. Introduction

With the continuous development of the automotive industry and aerospace field, research on graphene-reinforced aluminum composite has gradually emerged. The hot extrusion process used in the preparation of light alloy-based composite has received much attention because of its ability to refine grains, increase density, affect the directional alignment of reinforcing phases along the extrusion direction (Ref 1-6), and substantially improve the strength and toughness of composite.

Shao (Ref 7) prepared GO (or GNPs)/5083Al composite by ball milling combined with pressure infiltration, and the composite properties were further enhanced by hot extrusion to obtain a high tensile strength. Yang (Ref 8) noted that the matrix grains were refined to a greater extent after extrusion compared to the coarse grains produced by hot-pressing. The presence of fine grains usually indicates the occurrence of dynamic recrystallization (DRX) (Ref 9, 10). Studies on the influence of microstructure evolution of composite after hot extrusion have shown that finer grains are generated by nucleation mechanisms excited by uniformly dispersed reinforcing particles (Ref 11, 12). Wang (Ref 13) conducted hot extrusion experiments on magnesium matrix composite reinforced with 10 wt.% TC4 (Ti-6Al-4 V) particles, and the results showed that hot extrusion promoted a uniform distribution of $Mg_{17}Al_{12}$ in the matrix, eliminated the segregation of TC4 particles at the grain boundaries, reduced the stress concentration in the composite, and finally, obtained TC4/AZ91 composite with a final strength of 369 MPa and an average elongation of 6.4, which is 48 and 2.4% higher than those of the composite before extrusion, respectively. Chen (Ref 14) improved the tensile properties and average elongation of 5 wt.% AlN particle-reinforced magnesium matrix composite resulting from the more uniform distribution of AlN particles in the matrix produced by hot extrusion. Yu (Ref 15) prepared 0.3 wt.% GNSs/Al6063 composite with a tensile strength of 276 MPa by mechanical ball milling combined with hot extrusion. The average elongation was 14%, which was the same as that of the aluminum alloy matrix prepared by the same process. In hot extrusion processes of light alloys and their composite (Ref 16-19), key extrusion parameters may influence the microstructure evolution and the mechanical properties of the extrudate. Extrusion temperature is one of the most important parameters that determines the plasticity of the material, plays key roles during the hardening and softening processes (caused by the dynamic recovery and recrystallization of the grains), and directly affects the performance of the extruded parts. Furthermore, extremely high temperatures may also give rise to abnormally coarse grains. For graphene nanoplatelet-reinforced aluminum composite (GNPs/Al composite), high temperatures may cause GNPs to react with the aluminum matrix to generate brittle phase Al_4C_3, which might degrade the properties of the composite at a relatively high percentage (Ref 20), indicating that extrusion temperature has an important influence on the properties of the GNPs/Al composite extrudate. However, few detailed studies associated with the effects of extrusion temperature on graphene-reinforced composite have been performed (Ref 21).

In this study, to obtain perfect properties of a 0.5 wt.% graphene nanoplatelet-reinforced aluminum (0.5 wt.% GNPs/

Shumei Lou, Baojia Cheng, Yongqiang Liu, Xin Li, Xuefeng Bai, Peng Chen, Yiming Li, and **Li Li**, College of Intelligent Equipment, Shandong University of Science and Technology, Tai'an 271000, China. Contact e-mail: skd992951@sdust.edu.cn.

Al) composite fabricated by hot-pressing, extrusion processes at five different temperatures were carried out. The effects of the extrusion temperature on the microstructure and mechanical properties of the composite were investigated to determine the optimal extrusion temperature for the 0.5 wt.% GNP/Al composite. At the optimal extrusion temperature, the extruded composite obtains the best mechanical properties, confirmed by the characterization analysis by OM, SEM, EBSD and TEM, which could provide a reference for determining the extrusion temperature in hot extrusions of graphene-reinforced aluminum composite.

2. Experimental

2.1 Preparation of the Composite

High-purity spherical aluminum powder (purity ≥ 99.98% and with an average particle size of 18 μm) was selected as the matrix, and GNPs (with a specific surface area of approximately 230 m^2/g and a sheet diameter of approximately 2-4 μm) were used as the reinforcement. The GNPs were ultrasonically dispersed in water, aluminum powder was added, and the mixture was then wet ball milled, vacuum hot-pressing sintered at 570 °C to obtain hot-pressed cylindrical 0.5 wt.% GNPs/Al composite billets with dimensions of Φ 42 × 30 mm. The detailed preparation process of the composite can be found in our previous work (Ref 3). The optical microscope (OM) image cut from a cross section inside the hot-pressed composite is shown in Fig. 1.

2.2 Hot Extrusion

The hot-pressed sintered cylindrical billets were subjected to hot extrusions on a 200-ton microcomputer-controlled servo-hydraulic press with a heating rate of 10 °C/min for the die, a holding time of 10 min, an extrusion speed of 1 mm/min, an extrusion ratio of 17:1, an extrusion die angle of A = 90°, and extrusion temperatures of 460, 470, 480, 490, and 500 °C. Accordingly, for convenience of description, the extruded composite at these five extrusion temperatures was named T-460 °C@GNPs/Al, T-470 °C@GNPs/Al, T-480 °C@GNPs/Al, T-490 °C@GNPs/Al, and T-500 °C@GNPs/Al. Figure 2 shows the density and the residual porosity of the composite before and after the extrusions, indicating that extrusion can improve the density and reduce the residual porosity. The extrusion temperature has little influence on the density and residual porosity of the composite.

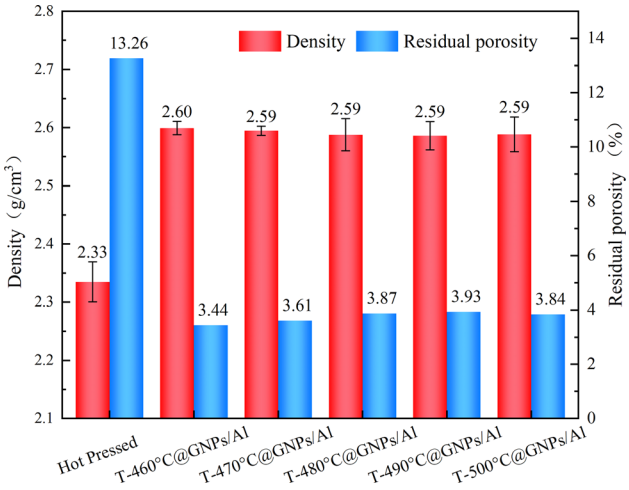

Fig. 2 Density and residual porosity of the composite before and after extrusion

2.3 Microstructure Characterization

The samples observed to character the microstructure were taken from the shaft sections parallel to the extrusion direction (ED).

The GNPs distribution was observed by an optical microscope. The GNPs and the composite were analyzed by Raman spectroscopy (Horiba Lab RAM HR Evolution) at a wavelength of 532 nm. The tensile fracture morphology of the composite was observed by field emission scanning electron microscopy (SEM, Sigma-300). The grain orientation and grain boundary distribution of the extruded composite were analyzed by electron backscatter diffraction (EBSD, FEIQuanta650F). The graphene distribution and GNP-Al interface structure in the GNPs/Al composite were characterized by field emission transmission electron microscopy (TEM, Talos F200X G2).

2.4 Mechanical Performance Tests

The microhardness of the composite on the shaft section, which is parallel to the ED, was tested by a microhardness tester (THVS-MA) with a test load of 25 g and a loading time of 10 s. The microhardness at five locations on each sample was measured. To ensure the accuracy of the data, the maximum and minimum values were removed, and the average value was adopted.

Tensile tests were carried out at room temperature using an electronic universal tensile testing machine (ZwickZ2.5TH). The average elongation and elastic modulus were measured by

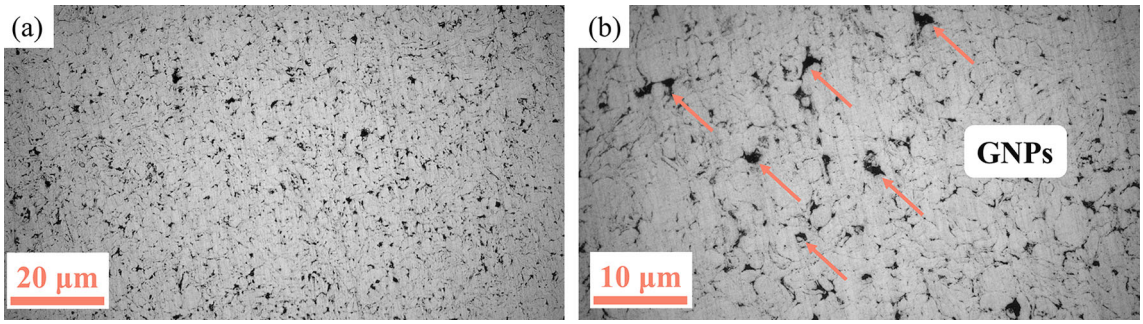

Fig. 1 OM image of the hot-pressed composite billet: (a) low magnification; (b) high magnification

a laser extensometer. The gauge length is 5 mm, and the tensile rate is 1 mm/min based on ISO 6892-1:2009, MOD. The length of the tensile sample is parallel to the ED (as shown in Fig. 3a) as well as the bending sample; the sizes of the tensile sample is shown in Fig. 3(b).

The three-point bending test of the composite was carried out at room temperature by using an electronic material testing machine (INSTRONE1000). A picture of the bending test and the dimensions of the bending sample are shown in Fig. 4.

To ensure that the measurement results are accurate and reliable, three samples are taken for each case.

3. Results and Discussion

3.1 Influence of Extrusion Temperature on the Microstructural Morphology of the Composite

3.1.1 Distribution of the GNPs. Figure 5 shows the optical morphology on the longitudinal section of the composite extruded at the five extrusion temperatures. Figure 5(a, c, e, g), and (i) shows that after hot extrusion, GNPs are arranged along the ED direction, and the GNPs in the composite are uniformly distributed without obvious agglomeration. The directional arrangement of the GNPs along the extrusion direction improves the tensile strength of the composite. From Fig. 5(b) and (d), it can be seen that there is a slight agglomeration of GNPs in the composite at extrusion temperatures of 460 and 470 °C. As the extrusion temperature increases, as shown in Fig. 5(f), (h), and (j), the agglomeration degree of the GNPs clearly decreases (Ref 3).

3.1.2 Raman Spectroscopy. Figure 6 shows the Raman spectra of the composite extruded at the five extrusion temperatures. For monolayer graphene, the value of I_{2D}/I_G is 4, and the 2D peak is unimodal (Ref 21, 22). With the increase in the number of GNP layers, the value of I_{2D}/I_G decreases, and the 2D peak is formed by the superposition of multiple subpeaks (Ref 23). First, Fig. 6(f) shows that the I_{2D}/I_G ratio of the GNPs increases from 0.58342 to 0.85871 with increasing extrusion temperature, indicating that the delamination of graphene is more obvious with increasing extrusion temperature. The increase in extrusion temperature can improve the fluidity of the aluminum matrix and delaminate the GNP layers, producing a stronger interface bond between the aluminum matrix and the GNPs. This is also indicated by the comparison between Fig. 5(b) and (j), in which the agglomeration degree of GNPs is higher at lower extrusion temperatures. Second, Fig. 6(f) shows that the I_D/I_G ratio of the T-460 °C@GNPs/Al composite is 1.8933. With increasing extrusion temperature, the I_D/I_G ratio first decreases and then increases. The lowest I_D/I_G ratio is 1.6227 for the T-480 °C@GNPs/Al composite. However, when the extrusion temperature is higher, the extremely large shearing stress caused by the large fluidity of the matrix will intensify the fracture of the GNPs, and at the same time, the increased temperature in some regions caused by the extreme deformation energy will promote the reaction between the GNPs and the aluminum, resulting in excess GNP defects. This indicates that a suitable temperature can ensure the fluidity of the matrix, thus decreasing the agglomeration and retaining the proper structural integrity of the GNPs.

3.1.3 Grain Orientation. Figure 7 shows the orientations and grain size distributions of the composite extruded at 460, 490 and 500 °C, and Fig. 8 shows the corresponding misorientation angle distributions. Figure 7 shows that the microstructure of the sample is mainly composed of grains elongated along the extrusion direction. In addition, sub-grain boundaries (the low misorientation angle shown in Fig. 8) always exist inside the grains, which is due to the high stacking fault energy of the aluminum matrix, and dynamic recovery more easily occurs. From the comparison of Fig. 7(a), (c), and (e), it can be seen that the grain orientation characteristics of the composite are most obvious when the extrusion temperature is 460 °C. This is because at low extrusion temperatures, the plasticity of the aluminum matrix and the fluidity are poor, and the effect of the dynamic recovery is weak, so work hardening plays a dominant role, and the proportion of low misorientation angles is 48.59% (the fraction of HAGBs is 51.41% in Fig. 8b). When the extrusion temperature rises, many equiaxed grains appear near the grain boundaries, which is mainly because the grain boundary itself could accumulate more dislocations, and the presence of graphene at the grain boundary aggravates this accumulation, which easily forms continuous dynamic recrystallization. At an extrusion temperature of 490 °C, more dynamic recovery (the fraction of HAGBs decreased to 48.24% in Fig. 8d) occurred, and then, continuous dynamic recrystallization began because of the higher extrusion temperature providing more energy for dynamic recrystallization. Figure 7(c) shows that many small-sized fine grains appear (also indicated by the percentage for the gain size of 2-3 μm in Fig. 8d), indicating that a great deal of continuous dynamic recrystallization occurs, which can increase the strength and plasticity of the composite.

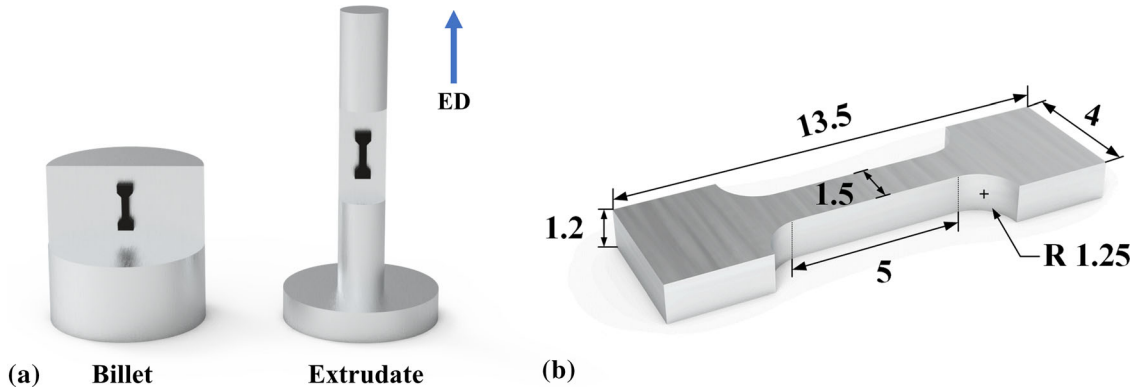

Fig. 3 Tensile sample at room temperature: (a) sampling location; (b) size (mm)

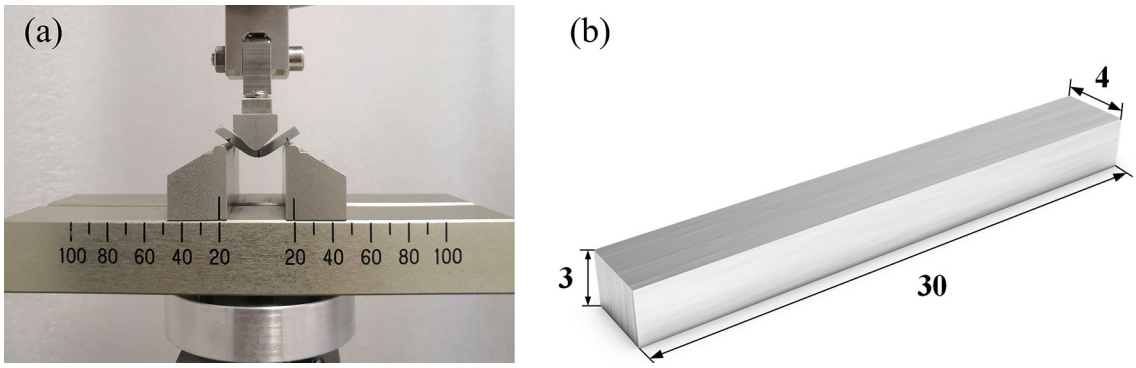

Fig. 4 Picture of the three-point bending test: (a) Three-point bending test; (b) Size of bending sample (mm)

However, as shown in Fig. 7(e), when the extrusion temperature is 500 °C, the fine grains produced by the continuous dynamic recrystallization of the composite grow (the average grain size reaches 5.34 μm), accompanied by the further generation of sub grains (the fraction of HAGBs decreases to 46.34% sequentially in Fig. 8f) due to the increase in the temperature.

3.2 Influence of the Extrusion Temperature on the Mechanical Properties of the Composite

3.2.1 Young's Modulus and Hardness. Figure 9 shows the Young's modulus for composite extruded at the five extrusion temperatures. The Young's modulus of the hot-pressed sintered composite is 41.09 GPa, mainly because the number of graphene layers in the hot-pressed composite is large and the van der Waals bonding force between the graphene layers is weak. The lower modulus perpendicular to the lamella (Ref 24), coupled with the agglomeration of GNPs, reduces the Young's modulus for the composite. The delamination of the graphene layers, the directional arrangement, the homodisperse of the GNPs, and the interfacial bonding strength between graphene and the matrix were improved by hot extrusion, leading to an increase in Young's modulus for the composite. The Young's modulus of the T-490 °C@GNPs/Al composite is 62.01 GPa, which is the highest and 51.91% higher than that of the hot-pressed composite.

Figure 10 shows the Vickers hardness of the composite at the five extrusion temperatures. It can be seen that the hardness of the hot-pressed composite is 31.08 HV, and the hardness of the composite increases greatly after the hot extrusions at the five temperatures. The hardness of the T-460 °C@GNPs/Al composite is 37.64 HV, and the maximum hardness is 45.5 HV at the temperature of 490 °C, which is 46.4% higher than that of the hot-pressed composite. The microstructure images near the indenter in Fig. 10 further indicate that the dispersion of the GNPs is improved and the number of layers are decreased in the composite extruded at 490 °C compared with the hot-pressed composite. The hardness of the T-500 °C@GNPs/Al composite decreases to 42.98, mainly due to the growth of aluminum grains.

3.2.2 Tensile Properties of the Composite. Figure 11 shows the representative tensile stress-strain curves at room temperature of the composite hot-pressed and extruded at the five extrusion temperatures, and the corresponding tensile properties are shown in Fig. 12. The tensile strength of the hot-pressed composite is 71.77 MPa, and the average elongation is 0.76% due to the relatively low hot-pressing temperature used to avoid too much reaction of the GNPs and the aluminum (Ref 3). The ultimate tensile strength and average elongation of the T-460 °C@GNPs/Al composite are 159.08 MPa and 19.41%, respectively. With increasing extrusion temperature, the ultimate tensile strength of the composite first decreases because the work hardening becomes weaker and then, increases to the highest tensile strength of 164.49 MPa, while the T-490 °C@GNPs/Al composite exhibits an average elongation of 21.81% because of the gain refinement resulting from the continuous dynamic recrystallization, the uniform distribution and delamination of the GNPs, as shown in Fig. 5 and 6. However, the tensile properties of the T-500 °C@GNPs/Al composite decrease owing to the decreased structural integrity of the GNPs (Fig. 6f) and grain growth (Fig. 7f).

3.2.3 Bending Properties of the Composite. Figure 13 shows the three-point bending curve of the composite hot-pressed and extruded at the five extrusion temperatures. The variation trend of the bending strength with the different extrusion temperatures is almost the same as that of the tensile strength (as shown in Fig. 11). The bending load and stiffness of the T-490 °C@GNPs/Al composite are the largest (the bending strength is 325.47 MPa).

From the above analysis, extrusion at lower extrusion temperatures brings a larger density and relatively large tensile strength because of work hardening; however, with the increase in extrusion temperature, the improved flow of the matrix brings more uniform and improved delamination of the GNPs, thereby improving the modulus, hardness and elongation of the composite. At 490 °C, the GNPs are uniformly dispersed, the delamination is perfect, and the structural integrity of the CNPs are the best. Furthermore, proper recrystallization results in proper grain refinement. Therefore, all the mechanical properties, including Young's modulus, hardness, tensile strength, bending strength, and average elongation of the T-490 °C@GNPs/Al composite, are the best. Based on the shear lag model of the composite (Ref 25), it can be concluded that when the extrusion temperature is 490 °C, the strengthening efficiency of hot extrusion on the 0.5 wt.% GNPs/Al composite is the highest. However, at 500 °C, the grain grows, and the structural integrity of the CNPs is destroyed, and almost all of the mechanical properties decrease.

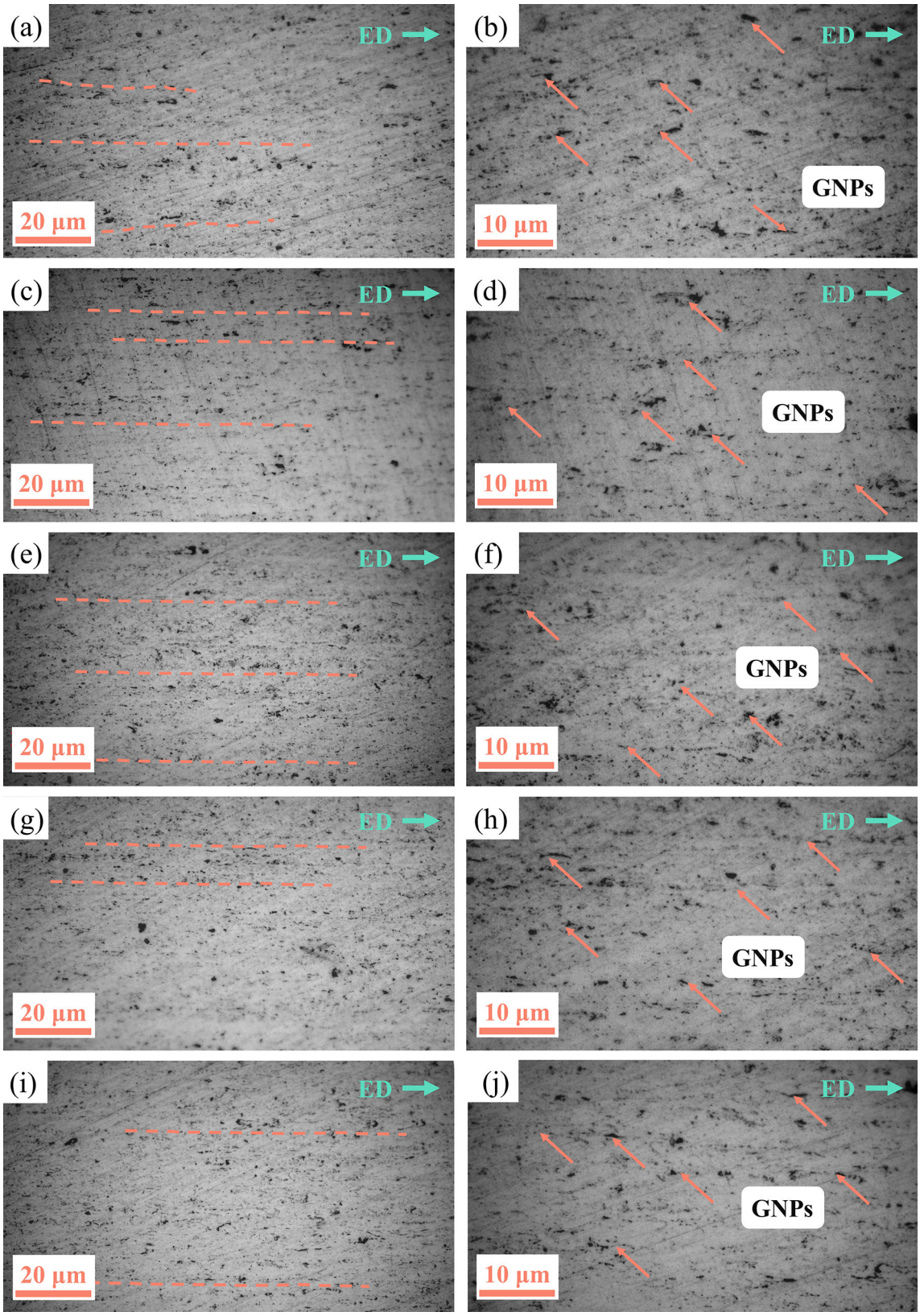

Fig. 5 OM image on the longitudinal section of the composite extruded at the five extrusion temperatures: (a), (b) T-460 °C@GNPs/Al; (c), (d) T-470 °C@GNPs/Al; (e), (f) T-480 °C@GNPs/Al; (g), (h) T-490 °C@GNPs/Al; (i), (j) T-500 °C@GNPs/Al

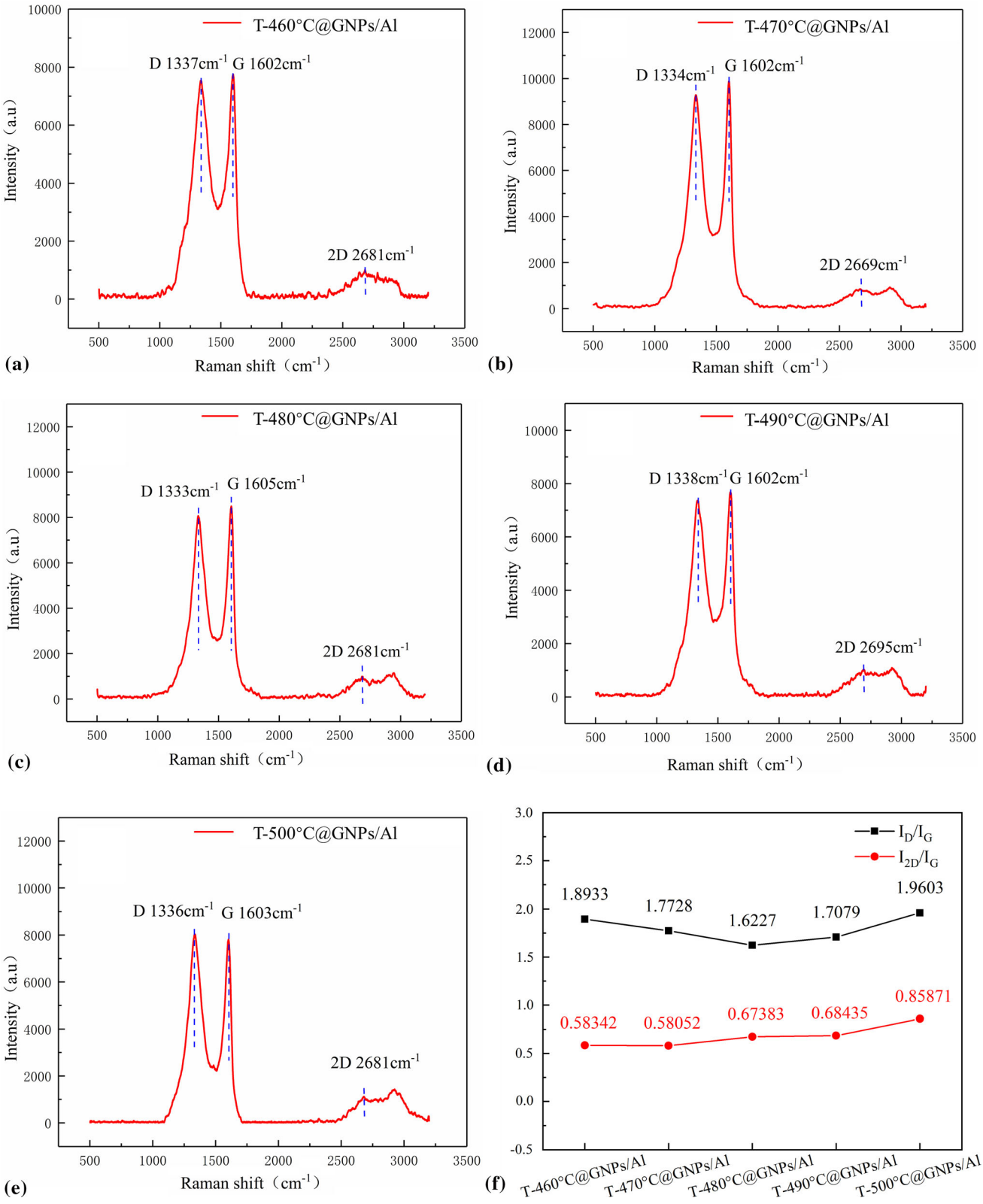

Fig. 6 Raman spectra of the composite extruded at the five temperatures: (a) T-460 °C@GNPs/Al; (b) T-470 °C@GNPs/Al; (c) T-480 °C@GNPs/Al; (d) T-490 °C@GNPs/Al; (e) T-500 °C@GNPs/Al; (f) I_D/I_G and I_{2D}/I_G ratios

3.3 Tensile Fracture Morphology

Figure 14 shows the SEM tensile fracture morphology of the composite hot-pressed and extruded at the five temperatures. To verify the distribution of the GNPs, an EDS mapping of the composite extruded at 490 °C is shown in Fig. 15. Figure. 14(b, d, f, h, j) and (l) shows magnifications of Fig. 14 (a, c, e, g, i) and (k), respectively. Figure. 14 shows that the

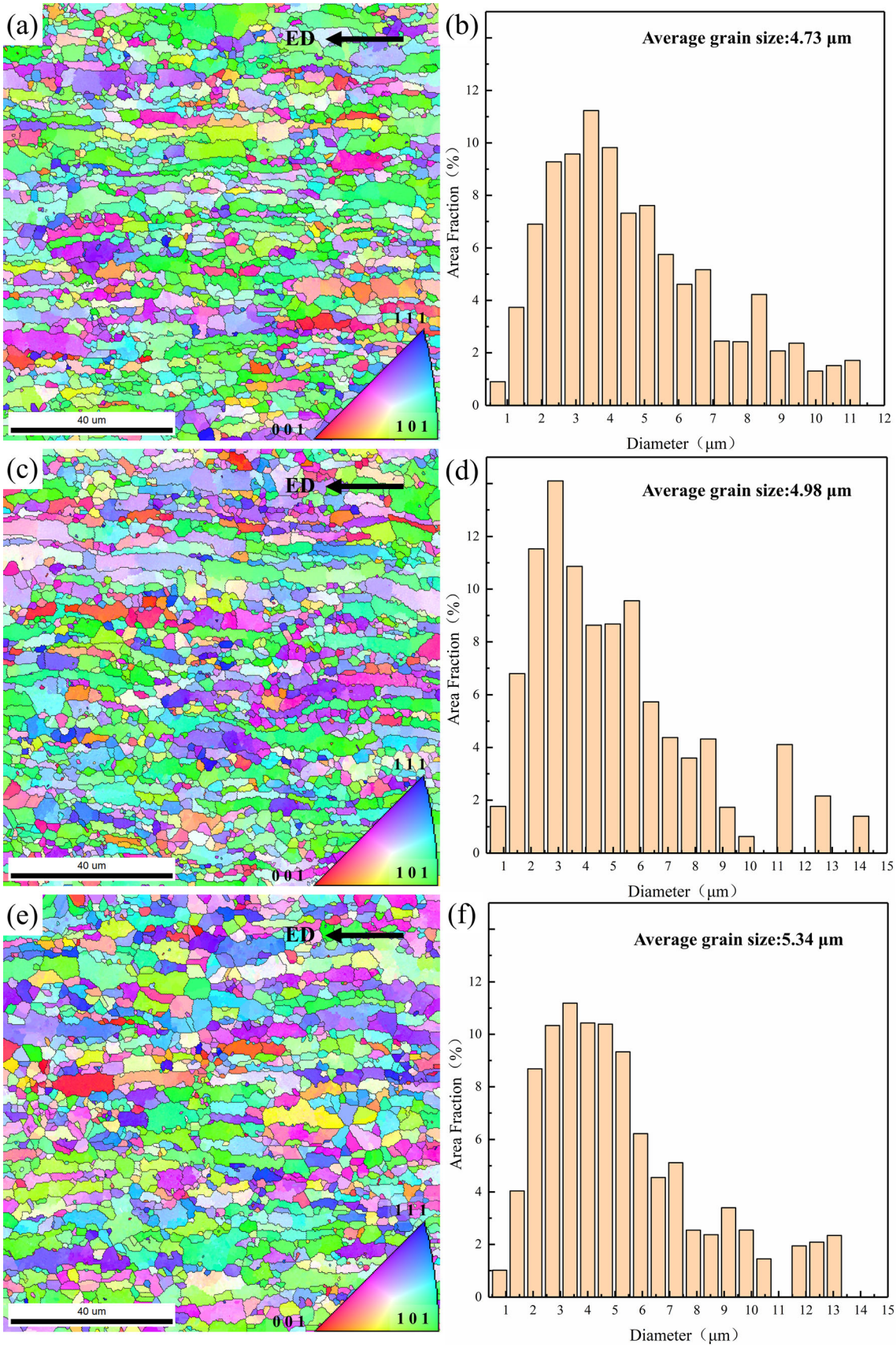

Fig. 7 Orientation and grain size distribution of the composite extruded at the different temperatures: (a), (b) T-460 °C@GNPs/Al; (c), (d) T-490 °C@GNPs/Al; (e), (f) T-500 °C@GNPs/Al

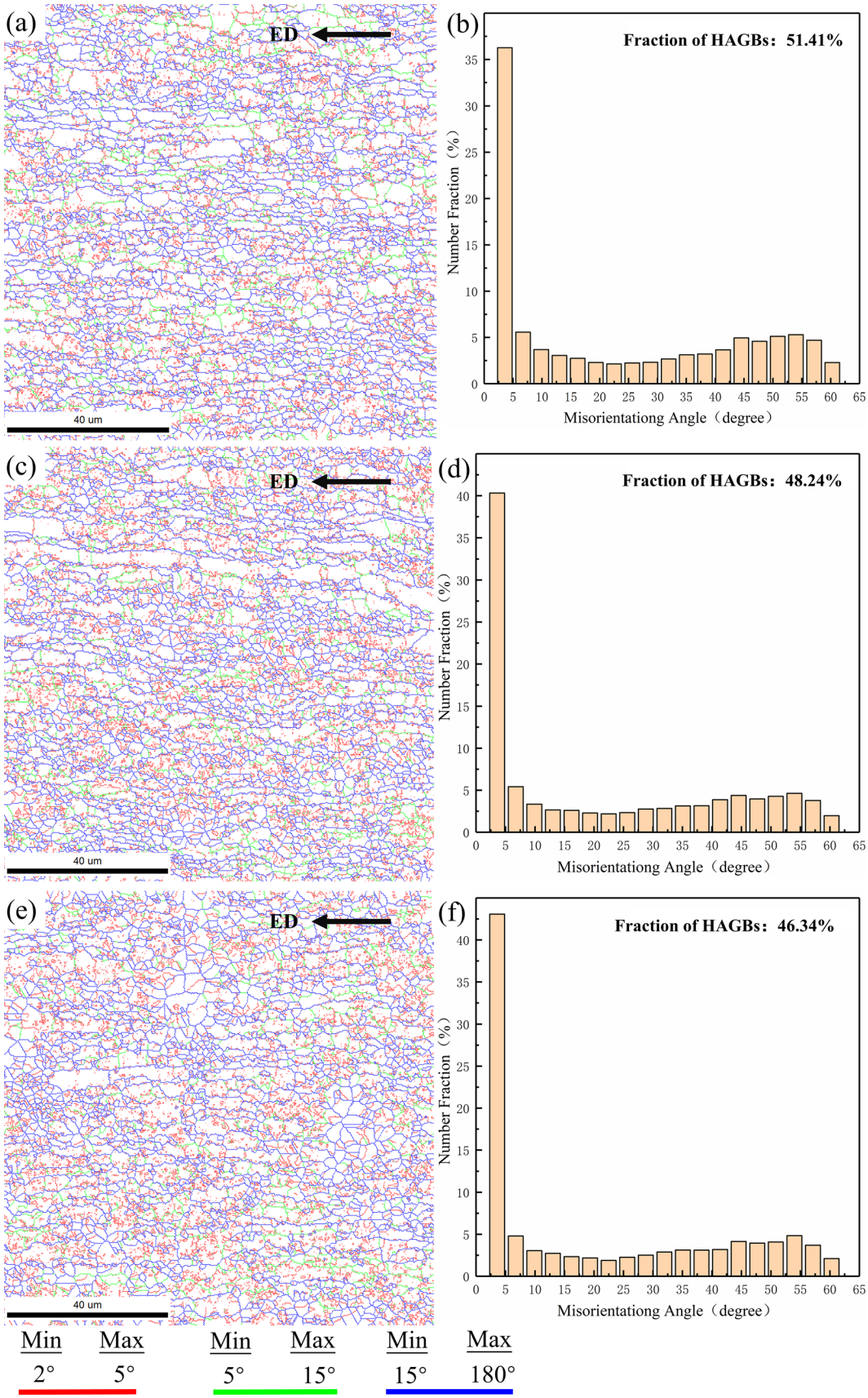

Fig. 8 Distribution of misorientation angle of the composite extruded at the different extrusion temperatures: (a), (b) T-460 °C@GNPs/Al; (c), (d) T-490 °C@GNPs/Al; (e), (f) T-500 °C@GNPs/Al

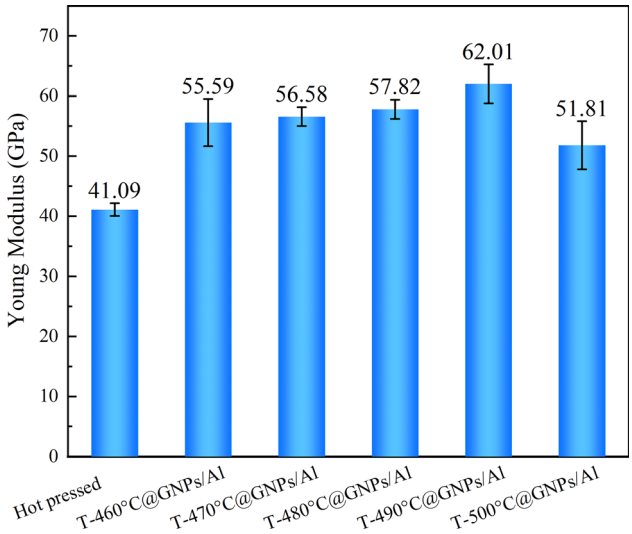

Fig. 9 Young's modulus of the composite hot-pressed and extruded at the five extrusion temperatures

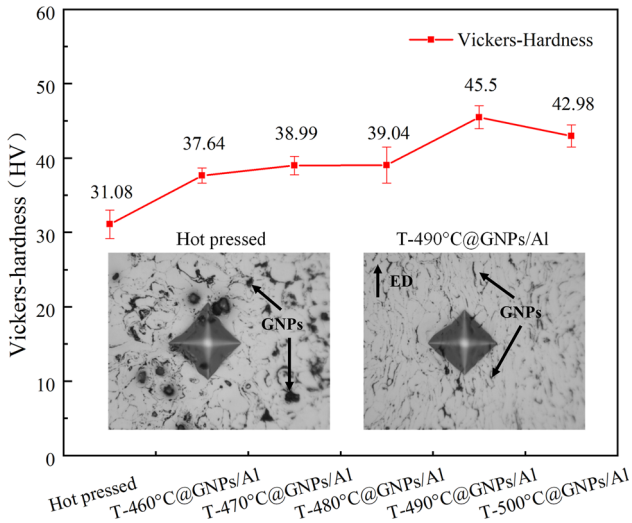

Fig. 10 Vickers hardness of the composite hot-pressed and extruded at the five extrusion temperatures

fracture morphology of the composite changed from brittle fracture (laminated cliff) to ductile fracture (dimple morphology) significantly after the hot extrusions: the dimples are equiaxed, deep, cup-shaped, and conical, exhibiting typical ductile fracture characteristics. As shown in Fig. 14(d), for the T-460 °C@GNPs/Al composite, the free GNPs in the dimples are in several layers. Additionally, the GNPs in the tearing edges are in multiple layers, resulting in relatively thick tearing edges. The weak van der Waals bonding force between the GNP layers and the poor interface bonding between the GNPs and the matrix contribute to crack initiation, forming large dimples and relatively worse mechanical performance (Fig. 9-Fig. 13). When the extrusion temperature increases, the number of GNP layers decreases, so the dimple is fine and uniform, while the tearing edge is thin and shiny (Fig. 14d, f, h, j and l). This is because, with the increase in extrusion temperature, the fluidity of the aluminum matrix increases, and the flow of the aluminum matrix will cause enough shear force, reducing the

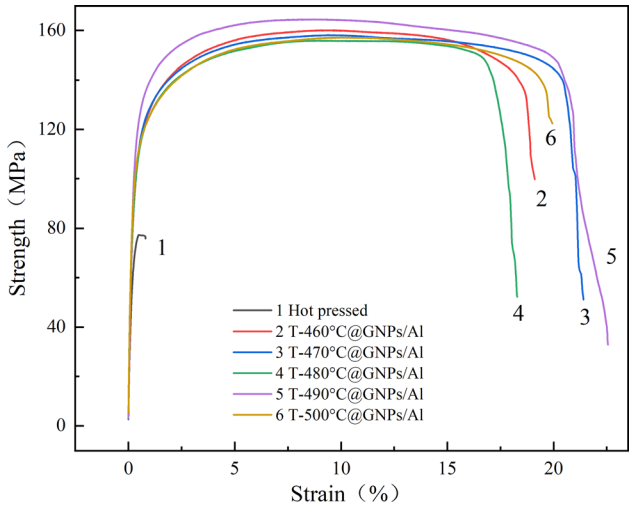

Fig. 11 Tensile stress-strain curves of the composite hot-pressed and extruded at the five extrusion temperatures

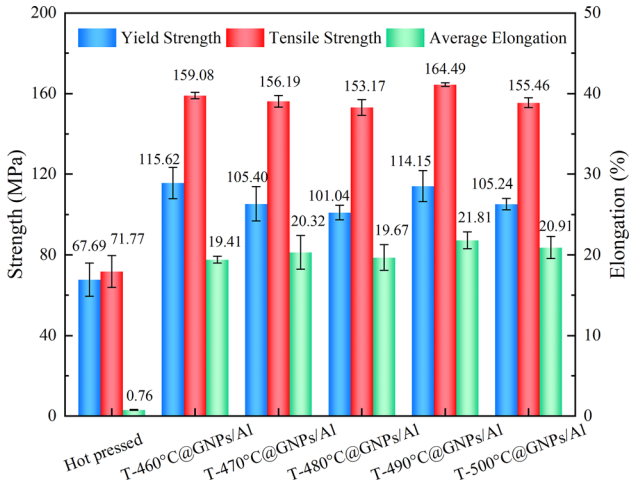

Fig. 12 Strengths and average elongation of the composite hot-pressed and extruded at the five extrusion temperatures

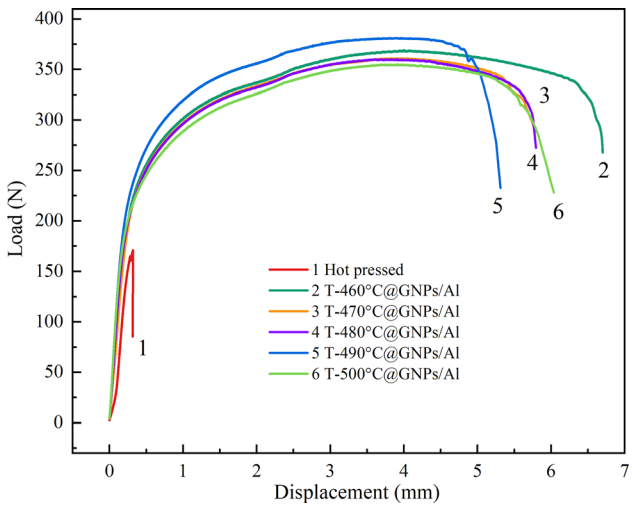

Fig. 13 Bending strength of the composite hot-pressed and extruded at the five extrusion temperatures

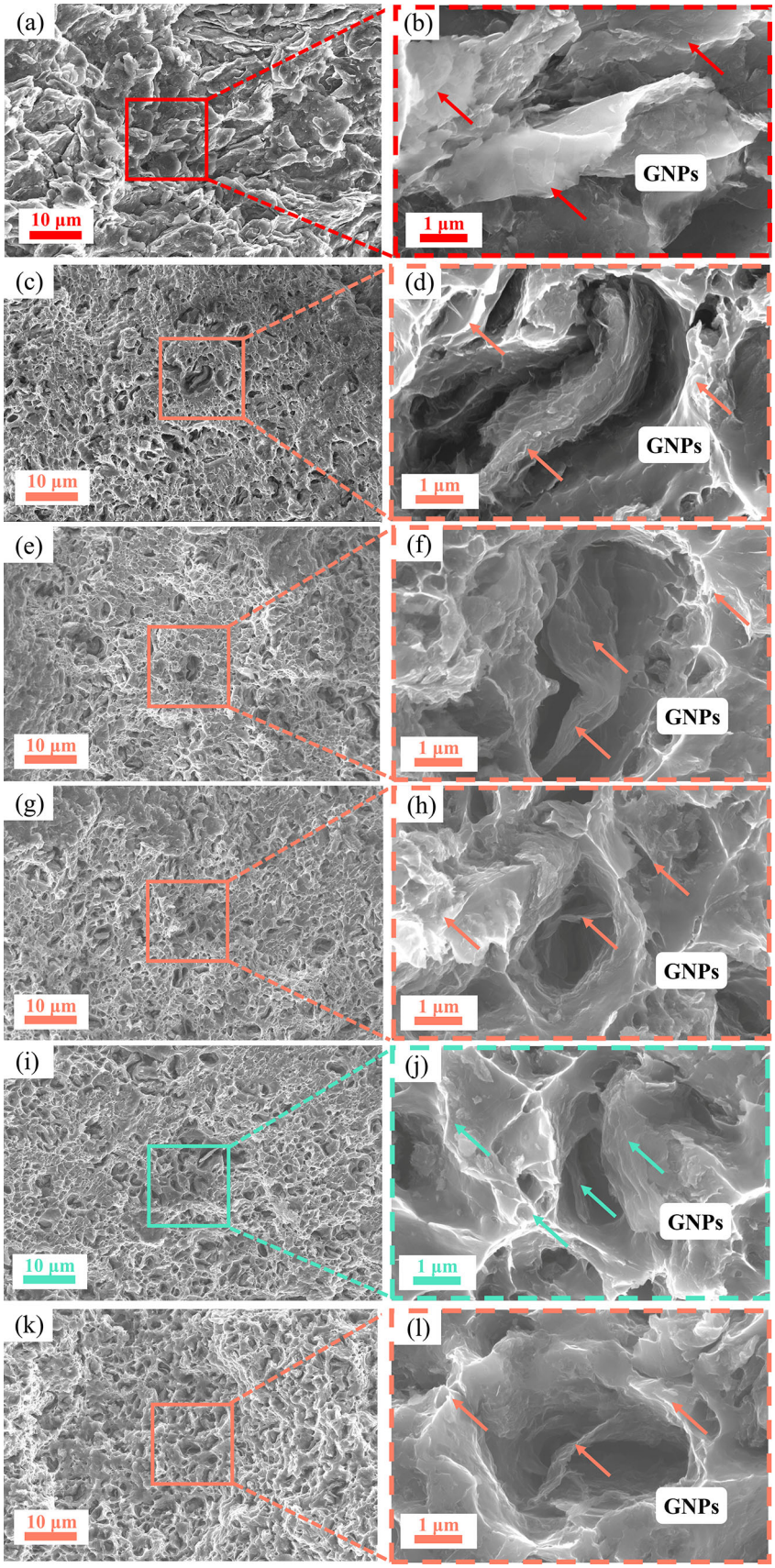

Fig. 14 Tensile fracture morphology of the composite hot-pressed and extruded at the five extrusion temperatures: (a), (b)Hot pressed; (c), (d) T-60 °C@GNPs/Al; (e), (f) T-470 °C@GNPs/Al; (g), (h) T-80 °C@GNPs/Al; (i), (j) T-490 °C@GNPs/Al; (k), (l) T-00 °C@GNPs/Al

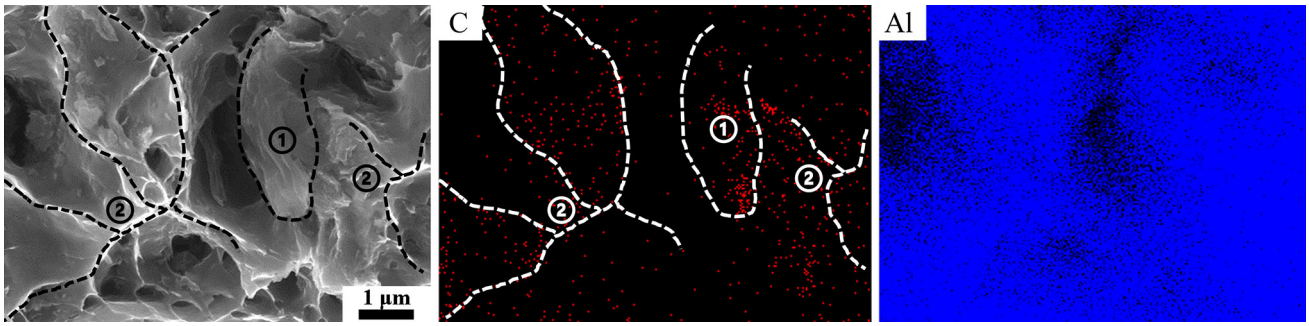

Fig. 15 EDS mapping of the composite extruded at 490 °C

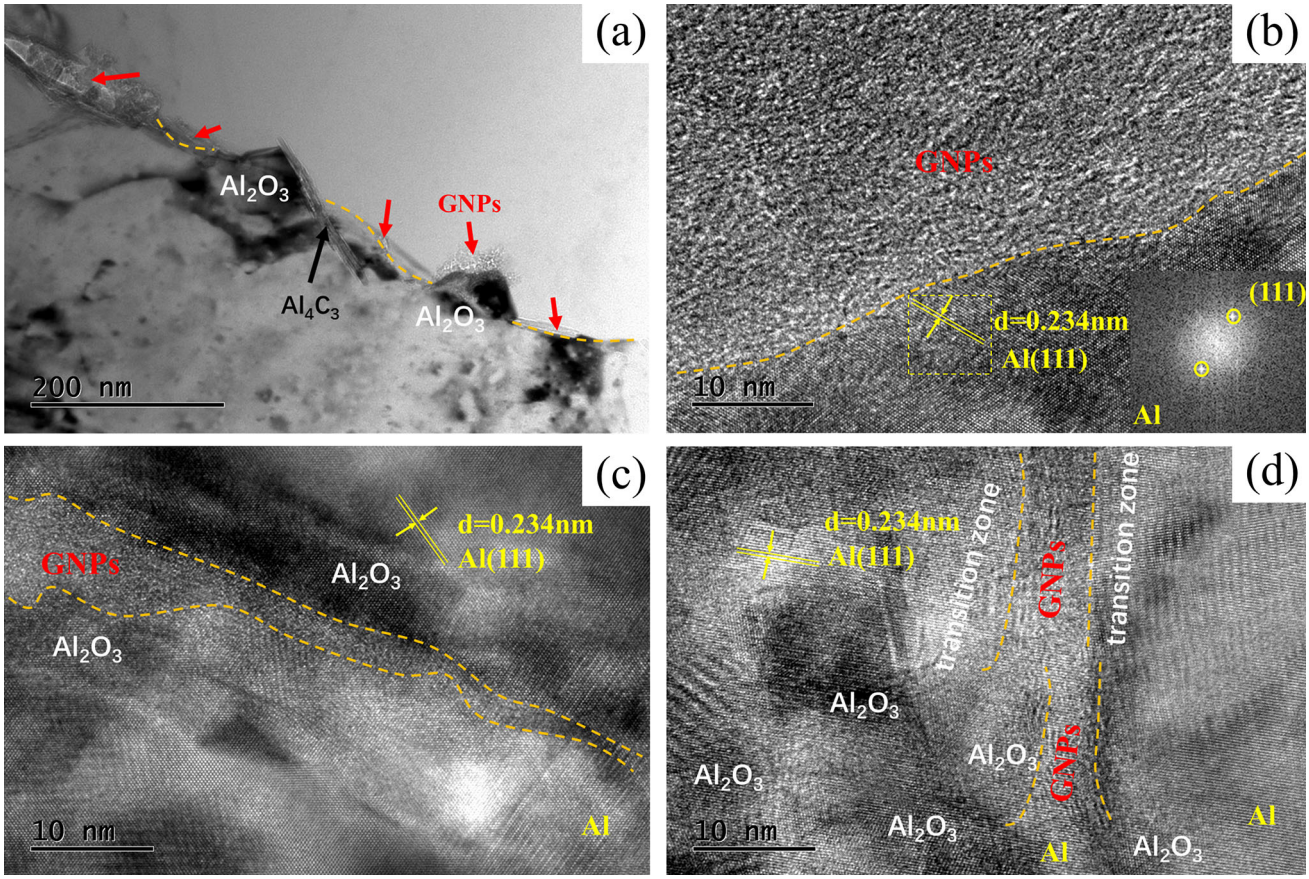

Fig. 16 Typical TEM images of GNP-Al interface structure in T-490 °C@ NPs/Al composite: (a) Al_4C_3 distribution and graphene distribution; (b), (c), (d) GNP-Al interface structure

number of GNP layers (as indicated in Fig. 14(i, j) and further indicated by ① in Fig. 15), and at the same time, increasing the bonding strength between the GNPs and aluminum matrix (as indicated in Fig. 14(i, j) and further indicated by ② in Fig. 15), resulting in a uniform fracture morphology (Fig. 14j) and the best mechanical performance at the extrusion temperature of 490 °C. At an extrusion temperature of 500 °C, the structural integrity of the CNPs is destroyed to some extent (as indicated by Fig. 6(f) and Fig. 14l), leading to a decline in the mechanical performance.

3.4 GNP-Al Interface

Figure 16 shows the typical interfaces of GNP-Al in the TEM image for the T-490 °C@GNPs/Al composite. It can be seen that GNPs are mainly dispersed at the grain boundaries, and an appropriate amount of Al_4C_3 shows a pinning effect on the grain boundaries of Al and GNPs, as shown in Fig. 16(a). The interface between the GNPs and the aluminum matrix exhibits different characteristics. One is the close mechanical bonding interface between Al and the GNPs (Ref 26), which is characterized by overlapping GNPs covering the aluminum

matrix. As shown in Fig. 16 (b), the Al (111) crystal plane forms a direct contact interface with the overlapping GNPs, and the crystal plane (111) acts as a typical slip plane of the aluminum matrix, indicating good wettability between Al (111) and the GNPs. The other is the indirect interface between Al and the GNPs participated in by amorphous alumina, as shown in Fig. 16(c). Alumina is broken and dispersed due to the shear friction of the extrusion and forms stable chemical bonds with graphene under the driving force of the Gibbs free energy change (Ref 27), which can effectively fix and compensate for interlayer slip. In addition, it was also found that the graphene exfoliated by extrusion shear was embedded in the aluminum matrix, which may cause defect nucleation and expansion by discontinuity, as shown in Fig. 16(e). The above results show that hot extrusion plays an important role in the delamination (Ref 28, 29) and good interface formation of GNPs and the matrix in GNPs/Al composite.

4. Conclusions

In this paper, the influence of extrusion temperatures on the microstructure and mechanical properties of 0.5 wt.% GNPs/Al composite is studied, and the following main conclusions can be drawn:

(1) The reinforcement of hot extrusion at different temperatures on the GNPs/Al composite is the combined effect of work hardening, dynamic recovery and dynamic recrystallization and the dispersion, delamination and structural integrity of the GNPs.
(2) When the temperature is low, work hardening results in a relatively high tensile strength, but because of the poor fluidity of the matrix, the dispersion and delamination of the GNPs by the extrusion is weak; as a result, the other mechanical properties are not as good. With increasing extrusion temperature, the dispersion and delamination of the GNPs and the effect of dynamic recrystallization gradually prevail the hard working, resulting in the best mechanical properties. When the extrusion temperature reaches 500 °C, grains grow and reduce the mechanical properties, and the overly high temperature could promote the reaction of the GNPs and the aluminum matrix, greatly reducing the structural integrity of the GNPs and then further decreasing the mechanical properties of the composite.
(3) The tensile fracture of the composite changed from brittle fracture to ductile fracture after hot extrusion at the five temperatures. Moreover, with increasing temperature, the dimple size decreases and becomes more uniform, the interface bonding between the GNPs and the aluminum matrix increases, and the tearing edges become thin and bright. However, when the temperature reaches 500 °C, the structural integrity of the GNPs declines, leading to a decrease in the mechanical properties of the composite.
(4) With the optimal extrusion temperature, a fine interface between the GNPs and the matrix is formed. GNPs are uniformly distributed in the aluminum matrix and are mainly dispersed at the grain boundaries, where some Al_4C_3 and Al_2O_3 exhibit pinning effects.

Acknowledgments

This study was funded by the Natural Science Foundation of Shandong Province, China (ZR2020KE013) and National Natural Science Foundation of China (No.51705295).

Conflict of interest

The authors declare that they have no conflict of interest.

References

1. M. Rashad, F. Pan, and M. Asif, Exploring Mechanical Behavior of Mg-6Zn Alloy Reinforced with Graphene Nanoplatelets, *Mater. Sci. Eng: A.*, 2016, **649**, p 263–269.
2. W. Li, Y. Liu, and G. Wu, Preparation of Graphite Flakes/Al with Preferred Orientation and High Thermal Conductivity by Squeeze Casting, *Carbon*, 2015, **95**, p 545–551.
3. S.M. Lou, Y.Q. Liu, C.D. Qu, G.X. Guo, L.W. Ran, P.P. Zhang, and C.J. Su, Influence of a Hot Extrusion with Rectangular-Section on Mechanical Properties and Microstructure of 0.5 wt% Graphene Nanoplate-Reinforced Aluminum Composite, *Adv. Eng. Mater.*, 2021, **23**, p 2001127.
4. M. Rashad, F. Pan, A. Tang, and M. Asif, Effect of Graphene Nanoplatelets Addition on Mechanical Properties of Pure Aluminum Using a Semi-Powder Method, *Prog. Nat. Sci: Mater. Int.*, 2014, **24**, p 101–108.
5. H. Zhang, C. Xu, W. Xiao, K. Ameyama, and C. Ma, Enhanced Mechanical Properties of Al5083 Alloy with Graphene Nanoplates Prepared by Ball Milling and Hot Extrusion, *Mater. Sci. Eng: A.*, 2016, **658**, p 8–15.
6. R. Deaquino-Lara, E. Gutiérrez-Castañeda, I. Estrada-Guel, G. Hinojosa-Ruiz, E. García-Sánchez, J.M. Herrera-Ramírez, R. Pérez-Bustamante, and R. Martínez-Sánchez, Structural Characterization of Aluminium Alloy 7075-Graphite Composite Fabricated by Mechanical Alloying and Hot Extrusion, *Mater. Des.*, 2014, **53**, p 1104–1111.
7. P. Shao, W. Yang, Q. Zhang, Q. Meng, X. Tan, Z. Xiu, J. Qiao, Z. Yu, and G. Wu, Microstructure and Tensile Properties of 5083 Al Matrix Composite Reinforced with Graphene Oxide and Graphene Nanoplates Prepared by Pressure Infiltration Method, *Compos. A*, 2018, **109**, p 151–162.
8. Q. Yang, D.L. Cheng, J. Liu, L. Wang, Z. Chen, M.L. Wang, S.Y. Zhong, Y. Wu, G. Ji, and H.W. Wang, Microstructure Evolution of the TiB2/Al Composites Fabricated by Powder Metallurgy During Hot Extrusion, *Mater. Charact.*, 2019, **155**, p 109834.
9. A. Güzel, A. Jäger, F. Parvizian, H.G. Lambers, A.E. Tekkaya, B. Svendsen, and H.J. Maier, A New Method for Determining Dynamic Grain Structure Evolution During Hot Aluminum Extrusion, *J. Mater. Process. Technol.*, 2012, **212**, p 323–330.
10. Z.C. Sun, L.S. Zheng, and H. Yang, Softening Mechanism and Microstructure Evolution of As-Extruded 7075 Aluminum Alloy During Hot Deformation, *Mater. Charact.*, 2014, **90**, p 71–80.
11. C. Schäfer, J. Song, and G. Gottstein, Modeling of Texture Evolution in the Deformation Zone of Second-Phase Particles, *Acta Mater.*, 2009, **57**, p 1026–1034.
12. J.D. Robson, D.T. Henry, and B. Davis, Particle Effects on Recrystallization in Magnesium-Manganese Alloys: Particle Pinning, *Mater. Sci. Eng: A.*, 2011, **528**, p 4239–4247.
13. X. Wang, X. Wang, X. Hu, and K. Wu, Effects of Hot Extrusion on Microstructure and Mechanical Properties of Mg Matrix Composite Reinforced with Deformable TC4 Particles., *J. Magn. Alloys*, 2020, **8**, p 421–430.
14. J. Chen, C. Bao, and F. Chen, Evolutions of Microstructure and Mechanical Properties for Mg-Al/AlN Composites Under Hot Extrusion, *Mater. Sci. Eng: A.*, 2016, **667**, p 426–434.
15. Z. Yu, W. Yang, C. Zhou, N. Zhang, Z. Chao, and H. liu, Y. Cao, Y. Sun, P. Shao and G. Wu, Effect of Ball Milling Time on Graphene Nanosheets Reinforced Al6063 Composite Fabricated by Pressure Infiltration Method, *Carbon*, 2019, **141**, p 25–39.
16. S. Li, I. Hisashi, K. Katsuyoshi, K. Akimichi, K. Yoshiharu, Y. Koji, and T. Motoi, Dependence of Microstructure and Mechanical Properties on Hot-Extrusion Temperatures of the Developed High-Strength

Cu40Zn-CrFeTiSn Brass by Powder Metallurgy, *Mater. Sci. Eng: A*, 2012, **558**, p 616–622.
17. S.L. Dong, B. Zhang, Y.L. Zhan, X. Liu, L. Xin, W.S. Yang, and G.H. Wu, Effect of Extrusion Temperature on the Microstructure and Mechanical Properties of SiCnw/2024Al Composite, *Mater.*, 2019, **12**, p 2769.
18. Q.H. Yan, Z.K. Xu, and D.H. Lu, Effects of Sintering Process and Hot Extrusion on Microstructures and Properties of Nano-Al_2O_{3p}/7075 Aluminum Matrix Composites, *Rare Met. Mater. Eng.*, 2021, **50**, p 3729–3738.
19. P. Zhao, L.D. Wang, Z.M. Du, S.C. Xu, P.P. Jin, and W.D. Fei, Low Temperature Extrusion of 6061 Aluminum Matrix Composite Reinforced with SnO2-Coated Al18B4O33 Whisker, *Compos. A*, 2012, **43**, p 183–188.
20. B. Guo, B. Chen, X. Zhang, X. Cen, X. Wang et al., Exploring the Size Effects of Al4C3 on the Mechanical Properties and Thermal Behaviors of Al Based Composites Reinforced by SiC and Carbon Nanotubes, *Carbon*, 2018, **135**, p 224–235.
21. P. Shao, G. Chen, B. Ju, W. Yang, Q. Zhang, Z. Wang, X. Tan, Y. Pei, S. Zhong, M. Hussain, and G. Wu, Effect of Hot Extrusion Temperature on Graphene Nanoplatelets Reinforced Al6061 Composite Fabricated by Pressure Infiltration Method, *Carbon*, 2020, **162**, p 455–464.
22. X. Gao, H. Yue, E. Guo, H. Zhang, X. Lin, L. Yao, and B. Wang, Preparation and Tensile Properties of Homogeneously Dispersed Graphene Reinforced Aluminum Matrix Composites, *Mater. Des.*, 2016, **94**, p 54–60.
23. H. Xu, X. Wu, X. Li, C. Luo, F. Liang, E. Orignac, J. Zhang, and J. Chu, Properties of Graphene-Metal Contacts Probed by Raman Spectroscopy, *Carbon*, 2018, **127**, p 491–497.
24. M.S. Dresselhaus, A. Jorio, M. Hofmann, G. Dresselhaus, and R. Saito, Perspectives on Carbon Nanotubes and Graphene Raman Spectroscopy, *Nano Lett.*, 2010, **3**, p 751–758.
25. X. Zhang, S. Zhu, H. Ding, Y. Bai, and P. Di, Fabrication and Properties of Hot-Pressing sintered WC-Al2O3 Composites Reinforced by Graphene Platelets, *Int. J. Refract. Met. Hard Mater.*, 2019, **82**, p 81–90.
26. B. Hou, P. Liu, A. Wang, and J. Xie, Interface Optimization Strategy for Enhancing the Mechanical and Thermal Properties of Aligned Graphene/Al Composite, *J. Alloys Compd.*, 2022, **900**, p 163555.
27. B. Ju, W. Yang, P. Shao, M. Hussain, Q. Zhang, Z. Xiu, X. Hou, J. Qiao, and G. Wu, Effect of Interfacial Microstructure on the Mechanical Properties of GNPs/Al Composites, *Carbon*, 2020, **162**, p 346–355.
28. X. Wang, W. Xiao, L. Wang, J. Shi, L. Sun, J. Cui, and J. Wang, Investigation on Mechanical Behavior of Multilayer Graphene Reinforced Aluminum Composites, *Phys. E.*, 2020, **123**, p 114172.
29. J. Zhu, X. Liu, and Q. Yang, Dislocation-Blocking Mechanism for the Strengthening and Toughening of Laminated Graphene/Al Composites, *Comput. Mater. Sci.*, 2019, **160**, p 72–81.